International Journal of Biological Macromolecules 132 (2019) 1304–1317

Contents lists available at ScienceDirect

International Journal of Biological Macromolecules

journal homepage: http://www.elsevier.com/locate/ijbiomac

Chitosan/nano-lignin based composite as a new sorbent for enhanced removal of dye pollution from aqueous solutions

Saima Sohni [a,b,*], Rokiah Hashim [a,*], Hafiz Nidaullah [a], Junidah Lamaming [a], Othman Sulaiman [a]

[a] School of Industrial Technology, Universiti Sains Malaysia, 11800 Minden, Penang, Malaysia
[b] Institute of Chemical Sciences, University of Peshawar, Peshawar, Pakistan

ARTICLE INFO

Article history:
Received 27 January 2019
Received in revised form 27 February 2019
Accepted 21 March 2019
Available online 26 March 2019

Keywords:
Chitosan/nano-lignin composite
Sorption
Methylene blue

ABSTRACT

The utilization of renewable and functional group enriched nano-lignin as bio-additve in fabricating composite has become the focus of attention worldwide. Herein, lignin nanoparticles in the form of hollow spheres with the diameter of the order of 138 ± 39 nm were directly prepared from agro-industrial waste (palm kernel shell) using recyclable tetrahydrofuran in an acidified aqueous system without any chemical modification steps. We then fabricated a new chitosan/nano-lignin composite material as highly efficient sorbent, as demonstrated by efficient removal (~83%) of methylene blue (MB) dye under natural pH conditions. The adsorption process obeyed pseudo-second-order kinetics and adequate fitting of the adsorption data using Langmuir model suggested a monolayer adsorption with a maximum adsorption capacity of 74.07 mg g^{-1}. Moreover, thermodynamic study of the system revealed spontaneous and endothermic nature of the sorption process. Further studies revealed that chitosan composite with nano-lignin showed better performance in dye decontamination compared to native chitosan and chitosan/bulk lignin composite. This could essentially be attributed to synergistic effects of size particularity (nano-effect) and incorporated functionalities due to lignin nanoparticles. Recyclability study performed in four repeated adsorption/regeneration cycles revealed recyclable nature of as-prepared composite, whilst adsorption experiments using spiked real water samples indicated recoveries as high as 89%. Based on this study, as-prepared bio-nanocomposite may thus be considered as an efficient and reusable adsorptive platform for the decontamination of water supplies.

1. Introduction

Bio-based chemicals and materials could easily be derived from fractions of the biomass that are apparently not suitable to yield food or biofuels, with the positive implication of enhancing the commercial viability of bio-refineries [1]. Lignin is the second most abundant non-food component of biomass next to cellulose and is considered as an unusual natural polyphenol with highly intricate structure [2]. The availability, non-toxicity, biodegradability, antioxidant property, antimicrobial nature, biocompatibility together with low cost makes lignin a significantly promising material for advanced applications such as, microfluidic devices, coating, glue, additives for natural rubber, drug delivery, wound healing, and antimicrobial materials [3,4]. Despite numerous scientific efforts, the exploitation of lignin as a renewable and cheap feedstock for different applications continues to remain a challenge till date, hence deserves consideration [5].

One of the interesting features related to lignin is the abundance of functional groups such as phenolic, carboxylic as well as aliphatic hydroxyl groups, providing the possibility for chemical modification and adjustment of polarity to develop compatibility with appropriate polymeric matrices [6]. On the other hand, chitosan-based materials have been intensively investigated in a number of fields such as wastewater treatment, separation membrane, food packaging, drug delivery and tissue engineering etc. [7–12]. The fabrication of chitosan-lignin based composite material has gained significant interest for multiple applications. For example, earlier Chen et al. prepared biodegradable chitosan/lignin films for potential usage as packaging films or wound dressings [13]. In another study, chitosan–lignin composites were explored as a promising adsorbent in wastewater decontamination [14]. Quite recently, the influence of lignin incorporation on the structure as well as functional properties of chitosan-based composite was investigated for application as packaging films [15,16]. Albadarin et al. fabricated activated lignin-chitosan extruded blend which were then characterized and used as sorbent for methylene blue (MB) dye removal [17]. However, the poor interfacial binding between bulk lignin and polymer matrix adversely affects its performance [18].

Furthermore, knowing that size particularity confers unique properties to nanomaterials [19], many researchers have started to investigate lignin at the nano- and macro- scale for prospective uses in numerous fields [20–25]. The fact that nanoparticles of polymer lignin (L_{NP}) are

* Corresponding authors at: School of Industrial Technology, Universiti Sains Malaysia, 11800, Penang, Malaysia.
E-mail addresses: saima.sohni@gmail.com (S. Sohni), hrokiah@usm.my (R. Hashim).

https://doi.org/10.1016/j.ijbiomac.2019.03.151
0141-8130/

biodegradable compared to synthetic inorganic nanoparticles and the possibility to prepare aqueous nanoparticle dispersions of L_{NP} in contrast to bulk lignin which is water insoluble makes it a fascinating candidate in fabricating new sustainable high performance bionanocomposite materials [26]. Few attempts have been made focusing on reinforcement of polymer composites using nano-sized lignin as bio-additive [6,20,27], nevertheless these studies are still in infancy and hence deserve scientific attention especially in the area of environmental remediation.

The growth of oil palm industry has been anticipated to remain strong in the next few decades with the consequence that the quantity of oil palm biomass waste generated will essentially remain high in the Southeast Asian countries, particularly in Malaysia [28]. One of the important residues is palm kernel shell (PKS) generated during palm oil extraction process. Predominantly used as low-rank solid fuel, there is a strong need to identify other downstream utilization routes for PKS that are more efficient and eco-friendly as the global trend to utilize lignocellulosic biomasses continue to diversify from their traditional usages. Earlier, we proposed that PKS can be exploited as a sustainable feedstock to fabricate various eco-friendly products due to substantially high lignin content found in these residues [29]. In the light of aforementioned details, this work is aimed to (i) synthesize L_{NP} directly from PKS biomass via. straightforward route using tetrahydrofuran (THF) that has been identified as renewable and biodegradable solvent for processing lignocellulosic biomass [30], (ii) and fabricate chitosan composite with L_{NP} (iii) as well as evaluate the performance of resulting bionanocomposite material as sorbent for the removal of MB, a cationic dye of widespread use in textile industries. To the best of our knowledge, present work is endeavoured to fabricate chitosan/nano-lignin composite material as an innovative sorbent for the removal of MB dye from aqueous solutions. We advocate that this study is going to provide a baseline for further studies to fabricate sustainable nano-lignin based composite materials for wastewater purification systems. The chemical structure of chitosan, and principal phenolic molecules that form possible lignin macromolecule are provided in Fig. 1 [22,31].

2. Experimental

2.1. Materials

All the reagents and chemical used were of analytical grade. In this study, PKS residues as shown in digital photographs in Fig. SI1 (see Supporting information) were collected in the year 2018 in August from United Oil Palm Industries, Nibong Tebal, Penang. The solvent THF used for the dissolution of lignin from PKS was purchased from QRec. Klason lignin powder was extracted from PKS using 72% sulphuric acid solution. The model dye (Table 1) used for present study was MB, Merck. All the chemicals were used as received. Deionized (DI) water was used in the study.

2.2. Methods

2.2.1. Facile route for the formation of nano-lignin

The sample of PKS biomass was air dried for a week followed by grinding to ~1.5 mm size using a knife mill (Riken Electric, RAB-15T11S3, CNS 2930). The procedure adopted for the extraction of lignin from PKS was the modified version of a report by Fukushima and Hatfield [33]. In a typical procedure, 5 g of PKS was transferred to round bottom flask. To this, THF (90 mL)-H_2SO_4 (10 mL of 2 N) was added and the suspension was refluxed for 30 min at 70 °C. Afterwards, the suspension thus obtained was filtered and THF was recovered using rotary evaporator, leaving behind a concentrated solution of dissolved lignin. This lignin rich liquid was added drop-wise (3 mL/min) to the flask containing warm DI water (200 mL) under slow stirring. In present work, immediate formation of L_{NP} took place facilely. Finally, obtained

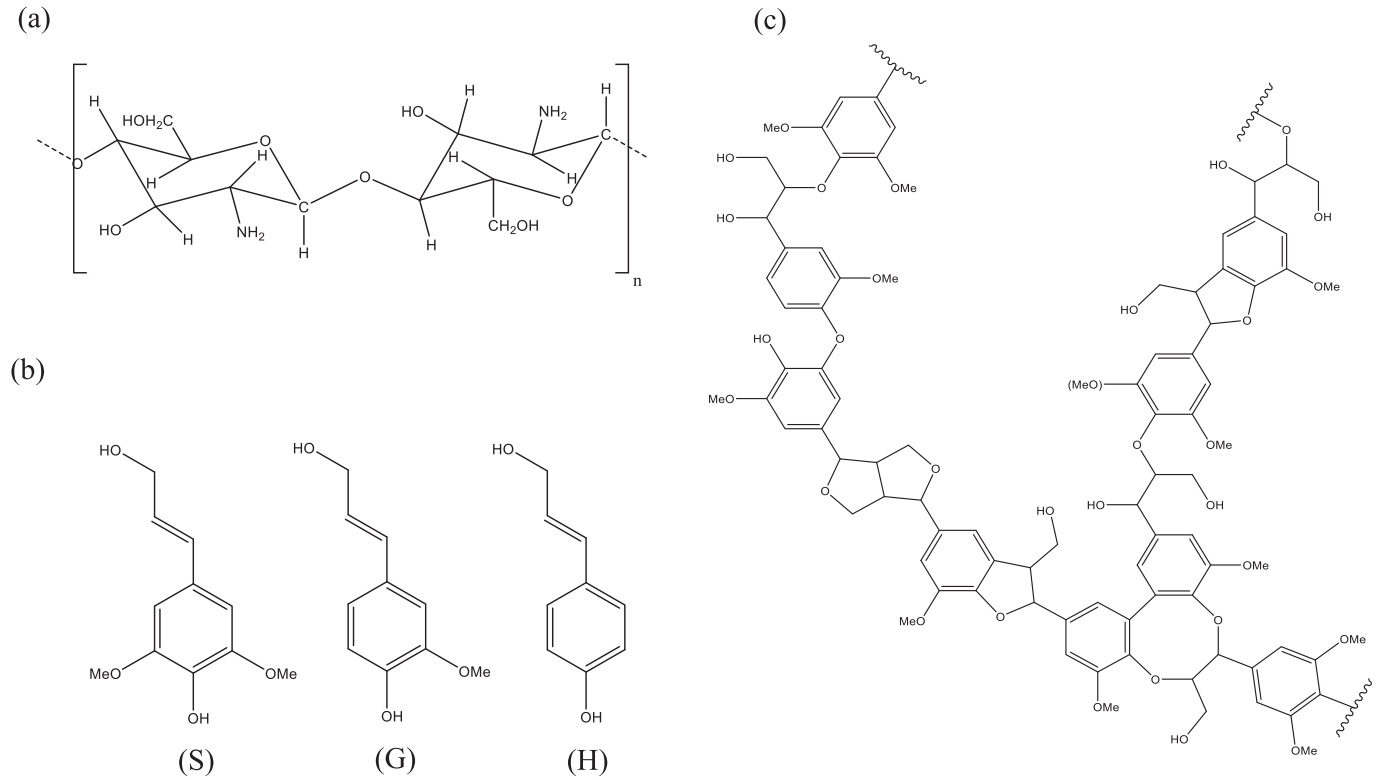

Fig. 1. (a) Chemical structure of chitosan, (b) three primary lignin monomers: sinapyl alcohol (syringyl, S), coniferyl alcohol (guaiacyl, G) and p-coumaryl alcohol (p-hydroxyphenol, H) and (c) lignin macromolecule.

Table 1
The information related to MB dye [32].

IUPAC name	Color index number	Maximum absorption wavelength	Formula	Molar mass	Class	Molecular structure
3,7-Bis(dimethylamino)phenazathionium chloride	52015	665 nm	$C_{16}H_{18}N_3$ SCl	319.85 g/mol	Phenothiazine	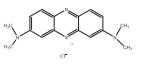

L_{NP} were washed, collected by centrifugation at 6000 rpm for 15 min and oven dried.

2.2.2. Fabrication of chitosan/nano-lignin composite

In brief, 2 g of chitosan was dissolved in 100 mL of 2% acetic acid solution under vigorous stirring, where the ketonic oxygen in the carboxyl group of an acetate molecule can make hydrogen bond with —OH groups of chitosan [34]. Next, L_{NP} (0.2 g) were added to this viscous chitosan solution and the resulting suspension was ultrasound dispersed for 30 min followed by stirring for 6 h. Prior to lyophilisation, the suspension of L_{NP} in chitosan was frozen at −21 °C using refrigerator for 24 h. Subsequently, the frozen suspensions were freeze dried at −47 °C for 48 h. The resulting chitosan/nano-lignin composite, henceforth designated as Chit/L_{NP}, was collected and washed with DI-water until the pH of washings reached 7. In parallel, chitosan-bulk lignin based composite was also prepared using klason lignin (0.4 g) for comparative analysis of the sorption performance towards model dye.

2.3. Characterization studies

The presence of different functional groups was established using Thermo Fisher Scientific (Nicolet iS50) Fourier-transform infrared (FTIR) spectrometer. For this purpose, potassium bromide and test material (5–10 mg) were pressed in the form of a pellet and absorption spectrum was recorded in the range of 4000–400 cm^{-1}. Information related to the morphologies of as-prepared L_{NP} and Chit/L_{NP} was acquired via scanning electron microscopy (SEM) performed using SEM Quanta FEG 450, USA. Using the Brunauer, Emmett and Teller (BET) equation, surface area of as-prepared composite was calculated from N_2 adsorption measurements performed at liquid N_2 temperature (77 K) by surface and pore analyzer micrometics ASAP 2020. Thermogravimetric analysis was performed on thermogravimetric analyzer (Model: TGA/DSC1 Star System, Mettler Toledo) under N_2 with a heating rate of 10 °C min^{-1}.

2.4. Evaluation of dye removal efficiency of as-prepared Chit/L_{NP} composite

The adsorption experiments were conducted in batch mode by adding known quantities of Chit/L_{NP} sorbent into conical flasks containing known concentration of MB dye solutions. Residual concentration of MB dye in the supernatant solution was analyzed by ultraviolet–visible (UV–VIS) spectrophotometer (Shimadzu UV-1601PC) at a wavelength of 665 nm and quantified using standard calibration curve (Figs. SI2 and SI3). The amount of MB dye adsorbed onto Chit/L_{NP} (q) and removal efficiency (%E) were calculated from the mass balanced equations given below;

$$q_e = (C_o - C_e)\,V/W \tag{1}$$

$$q_t = (C_o - C_t)V/W \tag{2}$$

$$\%E = \frac{C_o - C_e}{C_o} \times 100 \tag{3}$$

where C_o, C_e and C_t refer to the initial, equilibrium and concentration at time t of dye solution (mg L^{-1}) respectively, whilst V and W are the volume of dye solution (mL) and weight of sorbent material (mg), respectively [35].

2.4.1. Optimization of different parameters affecting sorption

It is well established that a number of factors are involved in controlling the uptake of adsorbate (dye in this study) by the sorbent material. Therefore, the influence of pH, contact time, dye concentration, among others was ascertained to optimize the removal of MB dye from aqueous solutions. The effect of solution pH was studied at initial concentration of 20 μg mL^{-1} of MB dye at pH values of 3, ~5 (natural), 7 and 9, adjusted by adding dilute solutions of NaOH and HCl. To understand the variation of adsorption with pH, evaluation of point of zero charge (pH_{pzc}) of composite was done by incubating sorbent material in a series of 0.01 M NaCl solution (50 mL) with pH adjusted by HCl (0.1 M) and NaOH (0.1 M) solutions [36]. Kinetic aspects related to dye uptake were also assessed over a range of 1 h to 48 h of contact time. The initial concentration of dye was varied from 20 to 120 mg L^{-1} to determine its effect on the adsorption capacity of Chit/L_{NP}-based composite.

2.4.2. Kinetic modelling and isotherms

The kinetics of sorption of MB dye from aqueous solution using Chit/L_{NP}-based composite were analyzed by four models, viz. pseudo-first-order, pseudo-second-order, intra-particle diffusion and Elovich models. The equation for pseudo-first-order kinetic model is represented by Eq. (4);

$$\log(q_e - q_t) = \log q_e - \frac{K_1 t}{2.303} \tag{4}$$

The equation representing pseudo-second-order kinetic model is provided below;

$$\frac{t}{q_t} = \frac{1}{K_2\, q_e^2} + \frac{t}{q_e} \tag{5}$$

where q_e and q_t correspond to the amount of adsorbed dye (mg g^{-1}) at equilibrium and at any given time, respectively. K_1 and K_2 refer to the pseudo-first- (min^{-1}) and pseudo-second- order rate constant (g mg^{-1} min^{-1}) of sorption process, respectively.

Data from kinetic study was also analyzed by intra-particle diffusion model (Eq. (6)) due to the inability of pseudo-first-order and pseudo-second-order kinetic models to identify diffusion mechanism.

$$q_{t=k_p t^{0.5}+C} \tag{6}$$

where k_p refers to intra-particle diffusion constant (mg g^{-1} $min^{-0.5}$) and C is the intercept (mg g^{-1}) related to the adsorption steps signifying boundary layer.

Another very useful model is the Elovich kinetic model which is based on the assumption that adsorbate is adsorbed on the solid surface without desorption, and the rate of adsorption drops with time due to an increased surface coverage. Following equation represents the Elovich model;

$$q_{t=\frac{1}{\beta}} \ln\alpha\,\beta + \frac{1}{\beta}\ln t \tag{7}$$

where α and β (gmg^{-1}) show initial sorption rate (mg g^{-1} min^{-1}), and desorption constant related to the extent of surface coverage and activation energy for chemisorption, respectively [37].

Equilibrium isotherm studies were performed to provide an insight into the surface properties, affinities and adsorption capacity of Chit/

L_{NP}-based composite as well as the distribution of dye molecules between aqueous phase and solid surface of the composite material. The Langmuir adsorption isotherm quantitatively describes the formation of a monolayer of adsorbate on the outer surface of adsorbent containing finite quantity of adsorption sites. The equation representing Langmuir isotherm is as follows;

$$\frac{C_e}{q_e} = \frac{1}{K_L q_o} + \frac{C_e}{q_o} \tag{8}$$

C_e (mg L^{-1}) signifies the equilibrium concentration of dye solution, q_e (mg g^{-1}) is the amount of dye adsorbed at equilibrium concentration, q_o (mg g^{-1}) refers to the maximum adsorption capacity and K_L corresponds to the Langmuir adsorption equilibrium constant (L mg^{-1}) which is related to energy of sorption. In addition, the Freundlich isotherm model as shown in Eq. (9) describes the adsorbate uptake on a heterogeneous surface that varies with surface coverage.

$$\ln q_e = \ln K_F + \left(\frac{1}{n}\right) \ln C_e \tag{9}$$

K_F ($mg^{1-1/n}$ $L^{1/n}$ g^{-1}) and n (dimensionless) correspond to the Freundlich constants related to adsorption capacity and surface heterogeneity, respectively [38].

2.4.3. Thermodynamic study

The effect of temperature on the interaction between MB dye and Chit/L_{NP}-based composite was assessed at selected temperature (303,

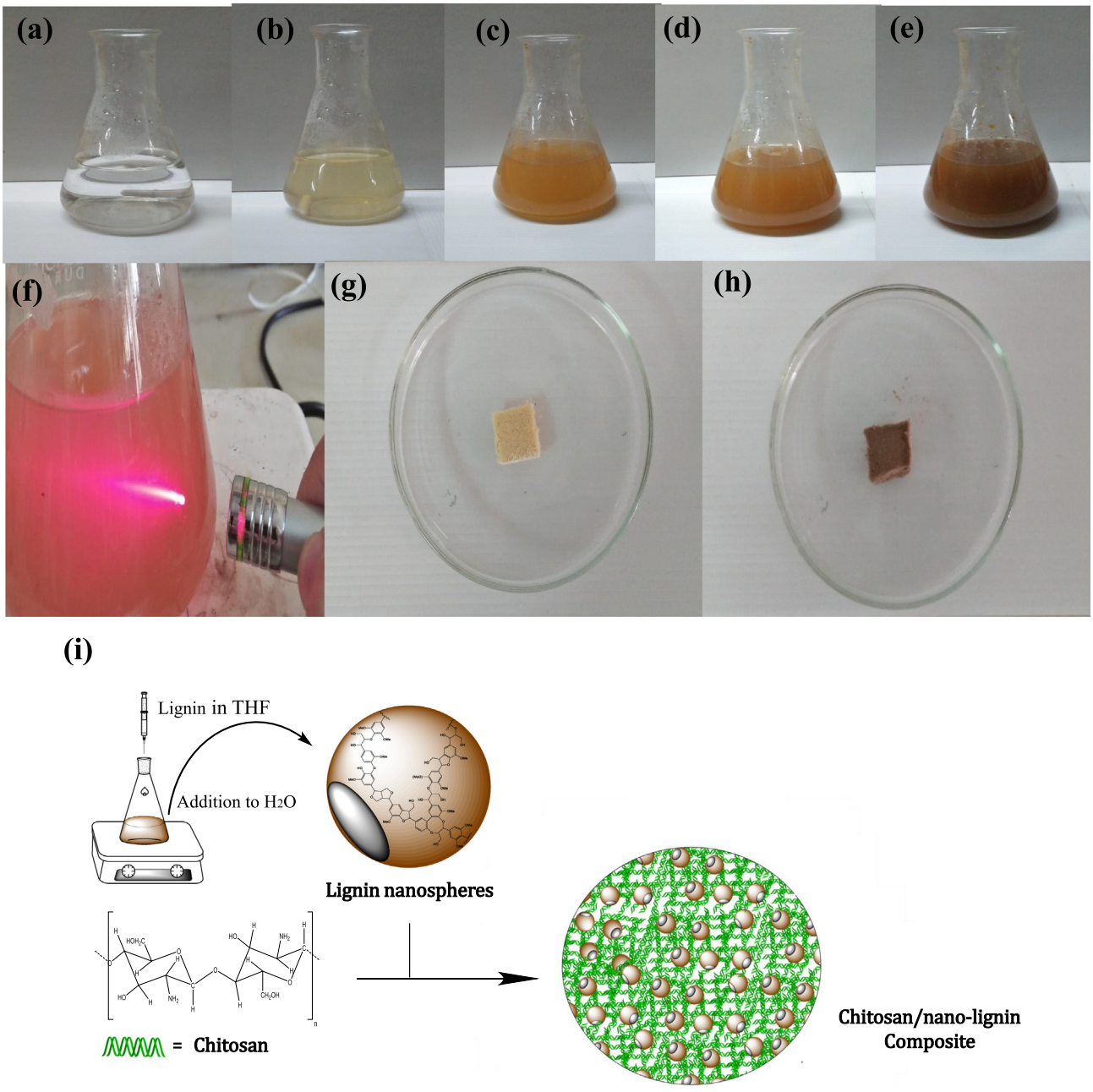

Fig. 2. Digital photographs showing formation of L_{NP} (a–e), scattering of laser light from the L_{NPs} suspension due to the Tyndall effect (f), chitosan (g) and Chit/L_{NP}–based composite (h), as well as illustration of hollow lignin nanospheres and Chit/L_{NP} formation (i).

323 and 343 K). The thermodynamic parameters, such as changes in free energy ($\Delta G°$, kJ mol^{-1}), enthalpy ($\Delta H°$, kJ mol^{-1}) and entropy ($\Delta S°$, kJ mol^{-1} K^{-1}) were calculated using following equations;

$$K_D = \frac{C_s}{C_e} \quad (10)$$

$$\Delta G^\circ = -RT \ln (K_D) \quad (11)$$

$$\Delta G^\circ = \Delta H^\circ - T\Delta S^\circ \quad (12)$$

$$\ln K_D = -\Delta H^0/RT + \Delta S^\circ/R = -\Delta G^\circ/\mathrm{RT} \text{ (van't Hoff equation)} \quad (13)$$

where K_D, C_s, R and T represent distribution coefficient, amount of dye adsorbed on the composite at equilibrium (mg L^{-1}), universal gas constant (8.314 J mol^{-1} K^{-1}) and absolute temperature (K), respectively. From the plot of ln K_D vs. 1/T, values of $\Delta H°$ and $\Delta S°$ can be derived from the slope and intercept, respectively, of the Van't Hoff plot [31].

2.5. Comparative study and application of Chit/L_{NP}-based composite to environmental aqueous samples

It was essential to understand the influence of inclusion of L_{NP} on the affinity of resulting composite material towards target pollutant. Hence, an identical experiment was run using chitosan, chitosan-bulk lignin based composite and Chit/L_{NP} as sorbents. For this purpose, a fixed

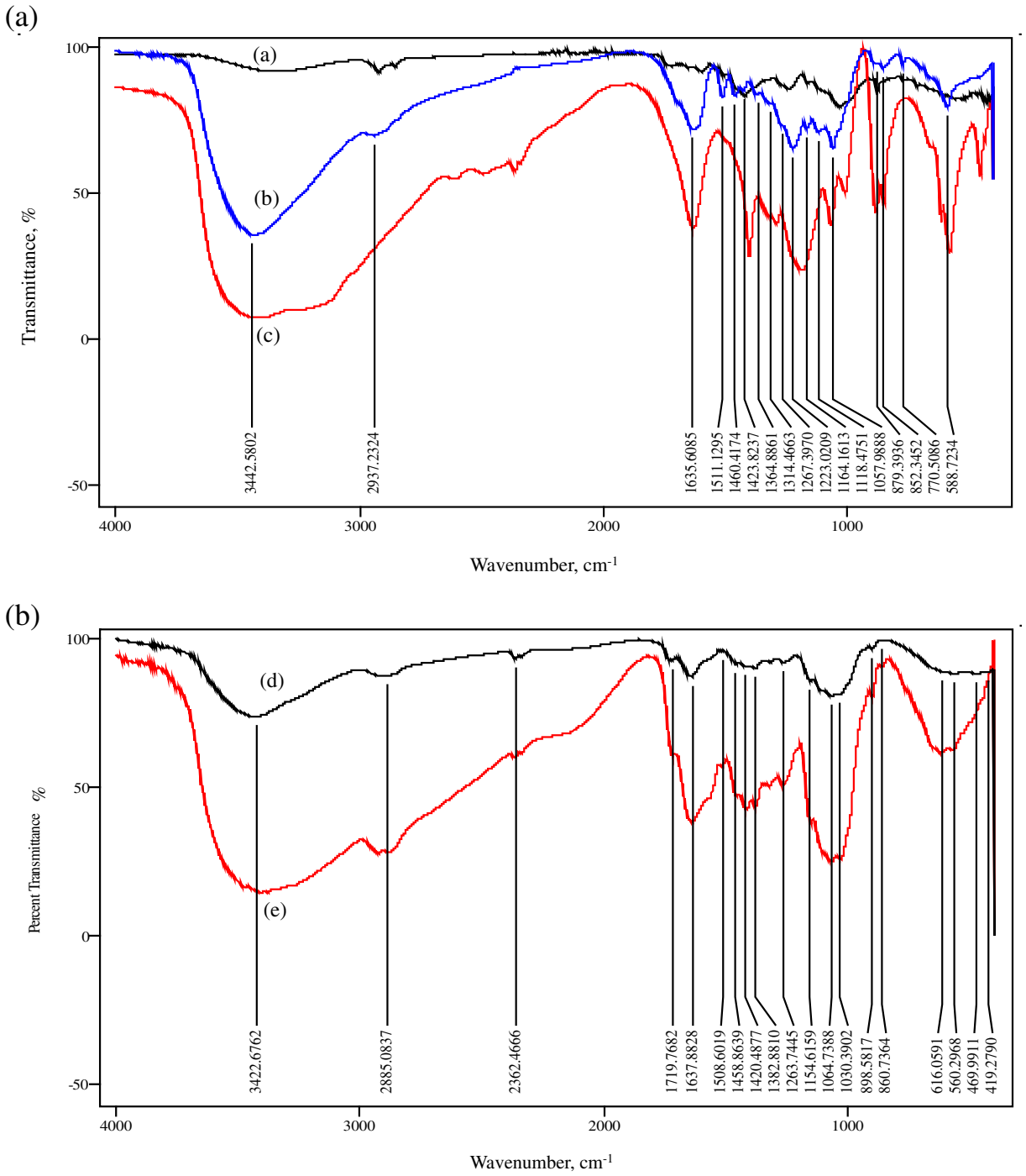

Fig. 3. FTIR spectra of PKS biomass (a), klason lignin (b) L_{NP} (c) chitosan (d) and Chit/L_{NP} (e).

dosage (10 mg) of each material was separately incubated in 20 μg mL^{-1} of dye solution (25 mL) at room temperature. In addition, the practical applicability of as-prepared composite material was assessed from the uptake of target pollutant from spiked real aqueous samples. Environmental samples were collected from different sources. A brief adsorption experiment was conducted by spiking these samples with 50 μg mL^{-1} of dye solution followed by adding a constant amount of Chit/L_{NP} (15 mg) in the test solution. The amount of MB dye removed from spiked samples was determined by comparing the concentration of dye prior to and after adding composite material.

2.6. Desorption and recyclability studies

To regenerate spent Chit/L_{NP} composite sorbent, desorption experiments were performed using distilled water and dilute hydrochloric acid solution as desorption solvent. In the next step, the regenerated Chit/L_{NP} composite was redirected for another round of adsorption experiments at room temperature in a total of 4 successive cycle of sorption-reuse.

3. Results and discussion

3.1. Preparation of Chit/L_{NP} composite material

In recent past, nanoscaled lignin has been prepared from acetylated alkali lignin [39], organosolv lignin fractions [22] and softwood kraft lignin [26]. In present work, L_{NP} in the form of hollow spheres of uniform morphology were directly prepared from PKS residue using a very simple synthesis approach without the involvement of any chemical modifications of the precursor. In addition, THF employed for the formation of L_{NP} was later recovered for reuse. Digital photographs showing formation of L_{NP} and also scattering of laser light from the colloidal system due to significant Tyndall effect are provided in Fig. 2a–f. In the next stage, Chit/L_{NP} composite was easily prepared, image shown in Fig. 2h, and characterized to understand the microscopic properties of as-prepared bionanocomposite.

3.2. Characterization of nanoscaled lignin and Chit/L_{NP} bionanocomposite

Different functional groups existing in raw PKS biomass, klason lignin and L_{NP} were identified on the basis of their absorption positions in their respective FTIR spectrum as compiled in Fig. 3. Detailed explanation of FTIR of PKS (Fig. 3a) in terms of peak assignment has been discussed in our previous work [29]. The FTIR spectrum of lignin (Fig. 3b) showed absorption bands at 3442.61 cm^{-1} (—OH stretching), 2966 cm^{-1} and 2937 cm^{-1} (C—H stretching of methyl and methylene groups), 1635 cm^{-1} (stretching of C═O conjugated to the aromatic ring), 1511 cm^{-1} (aromatic skeleton C—C stretching), 1460 cm^{-1} (C—H stretching of aromatic skeleton), 1423 cm^{-1} and 1364 cm^{-1} (bending of O—H of the phenolic group), 1267 cm^{-1} (C—O stretching vibration in G rings), 1223 cm^{-1} (C—O stretching vibration in S rings) and 1118 cm^{-1} (due to S units) and 1057.9 cm^{-1} (C—O stretching) [14,22]. As can be seen in Fig. 3c, main absorption bands in the FTIR spectrum of L_{NP} were roughly similar to that of lignin, implying that the chemical structure of nano-lignin did not change significantly. However certain differences that appeared might be due to the variations in the composition of klason lignin and L_{NP}, former containing residual carbohydrates and ash as impurities. The FTIR spectrum of chitosan provided in Fig. 3d showed absorption at ~3200 to 3700 cm^{-1} which can unambiguously be assigned to intra- and intermolecular stretching vibrations overlapped with N—H stretching, and another absorption band centred 2900 cm^{-1} due to symmetric and asymmetric C—H vibration. The peak positioned at 1637.91 cm^{-1} (bending of N—H of primary amine), small peaks at 1561 and 1544 cm^{-1} (bending of N—H of secondary amine), 1458 cm^{-1} (symmetrical deformation of CH_3 and CH_2 group), 1420 cm^{-1} due to C—N axial deformation (—NH_2 band), 1154 cm^{-1} due to (1–4)-glucosidic band in polysaccharide unit, 1099 cm^{-1} (stretching vibration mode of the —OH group) and

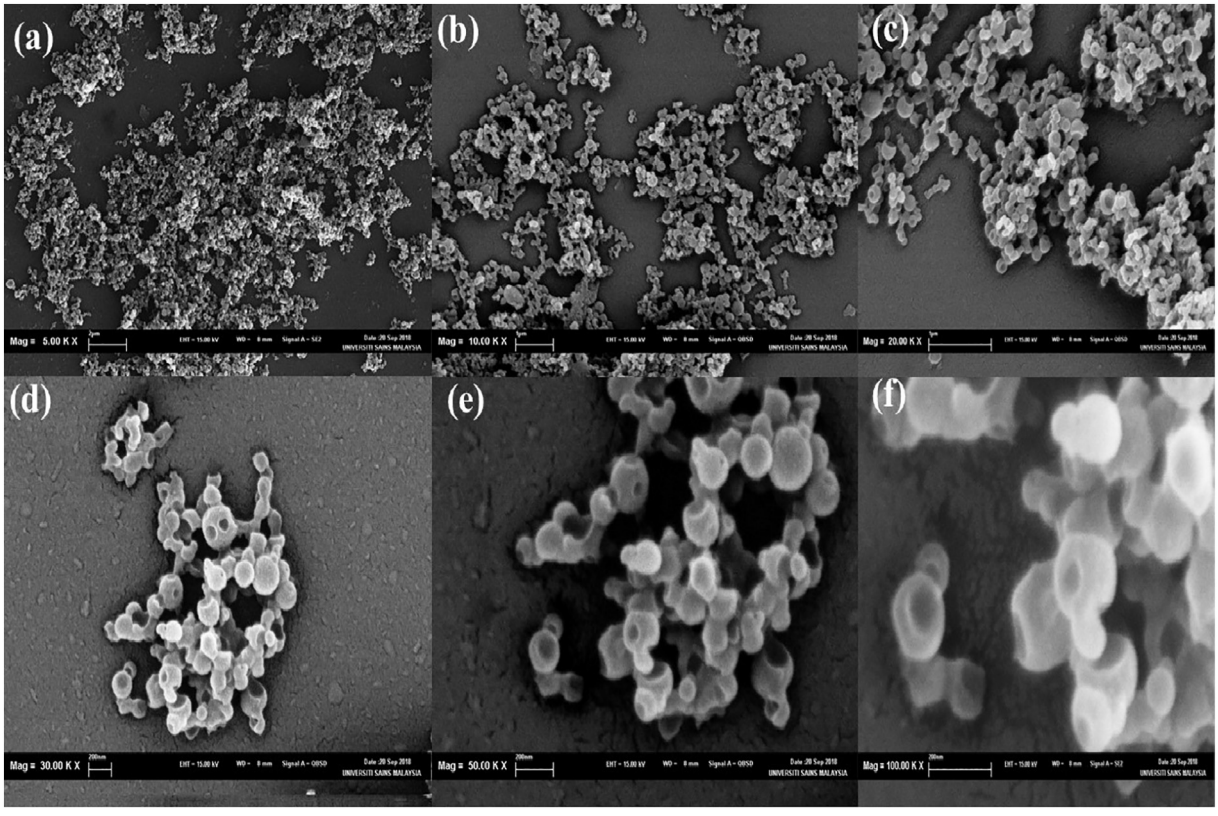

Fig. 4. SEM micrographs of L_{NP} at low (a–c) and high (d–f) magnifications.

1064.77 cm^{-1} (stretching vibration of C—O—C) were also seen [38]. An earlier work done by Chen et al. on chitosan/lignin composite films reported changes in the wavenumber in FTIR spectrum, implying obvious interactions between the two components [13]. In a recent work, it was stated that there are no strong interactions between lignin and chitosan, although a few low energy dipole−dipole interactions do exist, in particular involving carbonyl of chitosan and hydroxyl from lignin [15]. The FTIR spectrum of as-prepared composite revealed the occurrence of roughly all the functional groups of precursors (Fig. 3e), where measurable changes noticed in the absorption positions and changes in peak intensities due to different functional groups can account for the presence of weak interactions between the two entities. A small peak positioned at 1652 cm^{-1} (bending of N—H of primary amine) disappeared and peak at 1637.9 cm^{-1} (N—H stretching) shifted to a relatively broader peak at 1638.7 cm^{-1} in Chit/L_{NP}. Also, changes in the position and intensity were seen for N—H stretching centred at ~3400 cm^{-1}, this indicated the existence of certain interactions related to amine groups of chitosan in the formation of composite material. The disappearance of peak at 1652 cm^{-1} (bending of N—H of primary amine) as well as at 1561 cm^{-1} and 1544 cm^{-1} might be due to the interactions between aromatic ring of L_{NP} and amine group of chitosan. In Fig. 3d, peak at 1030.39 cm^{-1} (primary alcohol OH stretching) in the FTIR spectrum of chitosan appeared at 1029.71 cm^{-1} with reduced intensity in that of composite (see Fig. 3e). There were shifts noticed in the peaks due to C—O stretching from 1154.61 cm^{-1} in chitosan to a lesser intense peak at 1152.42 cm^{-1} in the composite as well, indicating the possibility of hydrogen bonding between functional groups of chitosan (amino, hydroxyl, carbonyl groups) and lignin (hydroxyl, carbonyl etc.) [14]. The presence of L_{NP} is going to increase the affinity of as-prepared material towards target pollutant because of the incorporated functionalities as confirmed from this study.

The SEM micrographs shown in Fig. 4a–f revealed chaplet-like lignin hollow symmetric nanospheres possessing single hole, with the dimension of 138 ± 39nm. It can be seen in the SEM images that L_{NP} exhibited uniform spherical and dense surface. These L_{NP} were formed as a result of hydrophobic aggregation of the polymeric chains in THF-H_2O dispersion medium, exhibiting hollow structure due to the effect of THF on the self-assembly behaviour. In principle, lignin can be completely dissolved in THF, however it forms a layer of membrane at two-phase interface when added to water. As the drop-wise addition continues, more and more lignin molecules aggregate at the internal surface of the membrane by self-assembly via π–π interactions. Finally, the thinner side of the membrane ruptures to maintain stable pressure inside and outside, leading to the formation of hole in the nanospheres [40]. On the other hand, microstructure of composite material showed rough and porous surface with embedded L_{NP} in polymer matrix of chitosan (marked with arrows in the SEM micrographs) as shown in Fig. 5. Nitrogen adsorption–desorption experiments were carried out to measure surface area and pore size of the composite (Fig. SI4a). As provided in Table 2, BET surface area for chitosan and Chit/L_{NP} were 3.44 and 2.39 m^2/g, respectively. BJH adsorption and desorption cumulative surface area of pores were 1.14 and 1.70 m^2/g, respectively for chitosan, and 0.58 and 0.69 m^2/g, respectively for Chit/L_{NP}. Adsorption and desorption average pore width are 41.16 and 32.79 Å, respectively for chitosan and corresponding values for composite are 87.42 and 85.86 Å, respectively. Apparently, the decrease in the surface area of chitosan after L_{NP} inclusion might be the result of blockage of chitosan porosities by incorporated L_{NP}. However, the interactions between different

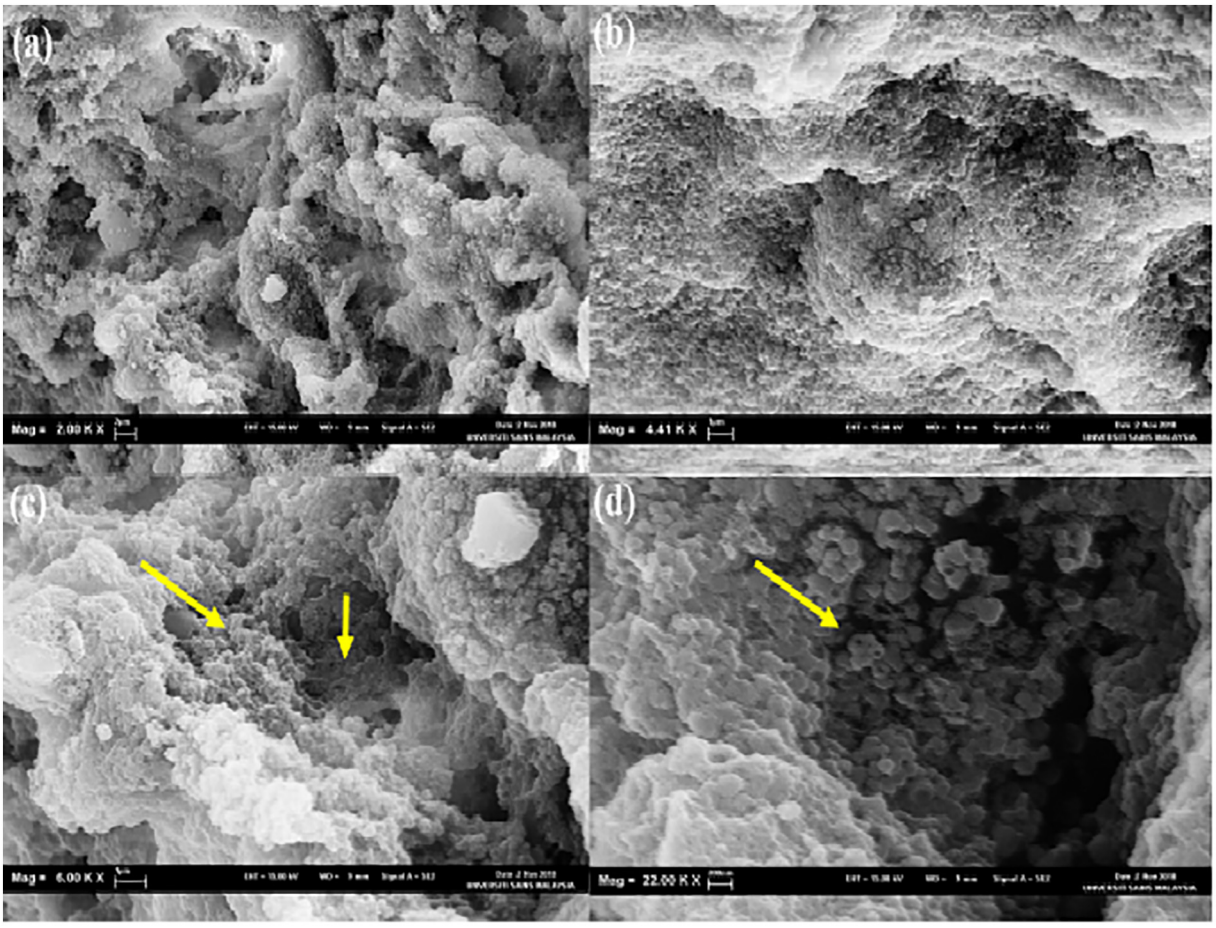

Fig. 5. SEM micrographs of Chit/L_{NP}–based composite at increasing magnifications.

functional groups such as —OH, C═O and —NH_2 on the surface of adsorbent favor pollutant uptake predominantly via chemisorption mechanism [41], hence enhanced dye removal can be anticipated. The effect of L_{NP} incorporation in chitosan matrix was assessed by comparing thermal stabilities of chitosan and Chit/L_{NP}, and the resulting thermogravimetric and differential thermogravimetric (TG/DTG) curves are shown in Fig. 6. In case of chitosan, TG curve presented weight loss as a function of temperature which is more obvious in the corresponding DTG curve (Fig. 6). Although TG/DTG curve for both materials were roughly identical, however the onset temperature for thermolytic process was higher in Chit/L_{NP} (268.76 °C) compared to native chitosan (257.41 °C), probably due to the stabilizing effect because of the inclusion of lignin nanospheres. The proportion of residue formed at 800 °C was higher in case of Chit/L_{NP} (30.20%) in comparison to chitosan (11.22%). The addition of L_{NP} into chitosan network forms a cross-linked and condensed matrix of aromatic structures at high temperatures, thereby leading to enhanced thermal stability of Chit/L_{NP} [14]. TGA analysis corroborated the results from FTIR and SEM analysis with regard to the formation of composite material.

3.3. Sorption of MB dye onto chitosan/nano-lignin composite

It is well known that adsorption capacity varies depending upon; (a) physical nature of sorbent and functional groups; (b) nature of the dye, its pK_a, functional groups, polarity, size and molecular weight, and (c) solution conditions (pH, time, dye concentration etc.) [42]. Therefore, optimization of various experimental conditions was performed in order to achieve optimal removal of target pollutant from test solutions and the relevant details have been discussed in the following sections.

3.3.1. Effect of solution pH

The effect of pH on removal efficiency of MB dye was studied in the range of pH 3 to 9 which revealed better solution decolonization at higher pH values, although uptake of MB dye was appreciable over extended pH range as shown in Fig. 7. This could be the outcome of strong adsorption and complexation interactions over wide pH range between composite and dyes via hydrogen bonding, electrostatic attraction, ion exchange and van der Waals force, etc. that stems from both components, i.e., chitosan (amino groups and hydroxyl groups) and L_{NP} (phenolic and aliphatic hydroxyl contents) of the Chit/L_{NP} composite [43]. In acidic solution (pH = 3), the dye removal efficiency was relatively lower, however, there was a rise in dye decontamination that remained somewhat stable (83–84%) with the increase of pH up to 9. At pH = 3, lower uptake of MB might be due to the electrostatic repulsion operative between protonated surface functional groups of composite and cationic dye molecule, leading to unfavorable adsorption [44]. In contrast, improvement in uptake of dye with increase in pH might be due to the increase in number of negatively charged sites (high concentrations of OH^- ions cause deprotonation) on sorbent, as a result augmenting the removal efficiency to 85% at pH = 9 [17]. In fact, these results are consistence with pH_{pzc} of Chit/L_{NP}, i.e. 2.4, much lower than the corresponding value for native chitosan (7.2) as provided in Fig. SI4b (see Supporting information). Further studies on the sorption of MB onto Chit/L_{NP} composite were carried out without any pH control which, we believe, is a very favorable aspect from practical application viewpoint.

Table 2
Surface area analysis.

Parameter	Chit/L_{NP}	Chitosan
BET surface area (m^2/g)	2.39	3.44
Langmuir surface area (m^2/g)	4.08	9.15
BJH Adsorption cumulative volume of pores (cm^3/g)	0.0064	0.0033
BJH Desorption cumulative volume of pores (cm^3/g)	0.0072	0.0043
Adsorption average pore width (Å)	87.42	41.16
Desorption average pore width (Å)	85.86	32.79

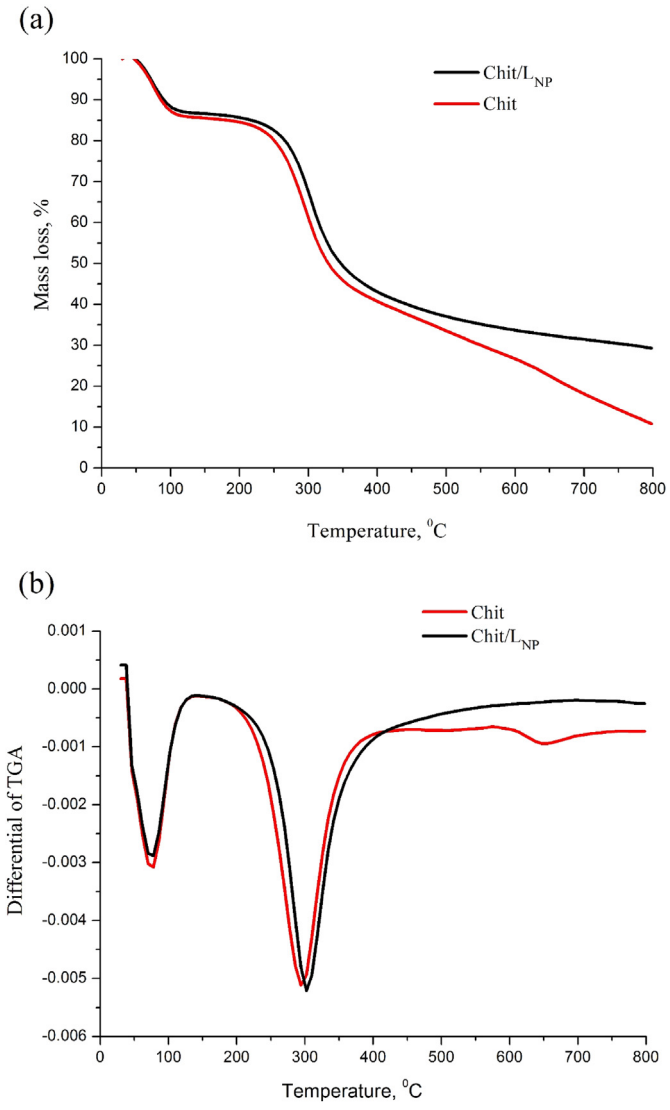

Fig. 6. TG and differential of TG for chitosan and Chit/L_{NP}.

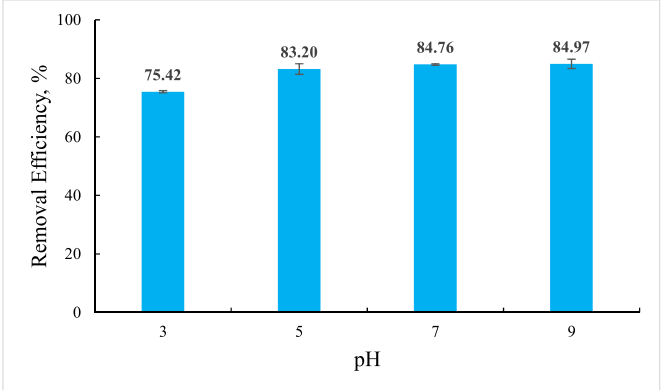

Fig. 7. Effect of pH on the sorption of MB dye onto Chit/L_{NP}-based nanocomposite. (Experimental conditions: sorbent = 10 mg, dye concentration = 20 μg mL^{-1}, volume = 25 mL, shaking speed = 150 rpm, room temperature.)

3.3.2. Effect of contact time

The effect of time on dye removal efficiency of as-prepared composite was investigated and the results are shown in Fig. 8a. The characteristic peak (λ_{max} = 665 nm) continued to decline in intensity and color of dye solution turned pale with time, and finally became colorless as can be seen in Fig. 8b. In the beginning of experiment, greater variations observed in the extent of adsorption can be attributed to the fact that all the sites on the surface of composite were predominantly vacant and the solute's concentration gradient was also high. Different aspects related to the mechanism of adsorption were evaluated by applying kinetic models to the experimental data such as pseudo first-order, pseudo-second order, intra-particle diffusion and Elovich kinetic models as presented in Fig. 8c–f. According to the data shown in Table 3, in case of pseudo-second order, R^2 value for model dye was

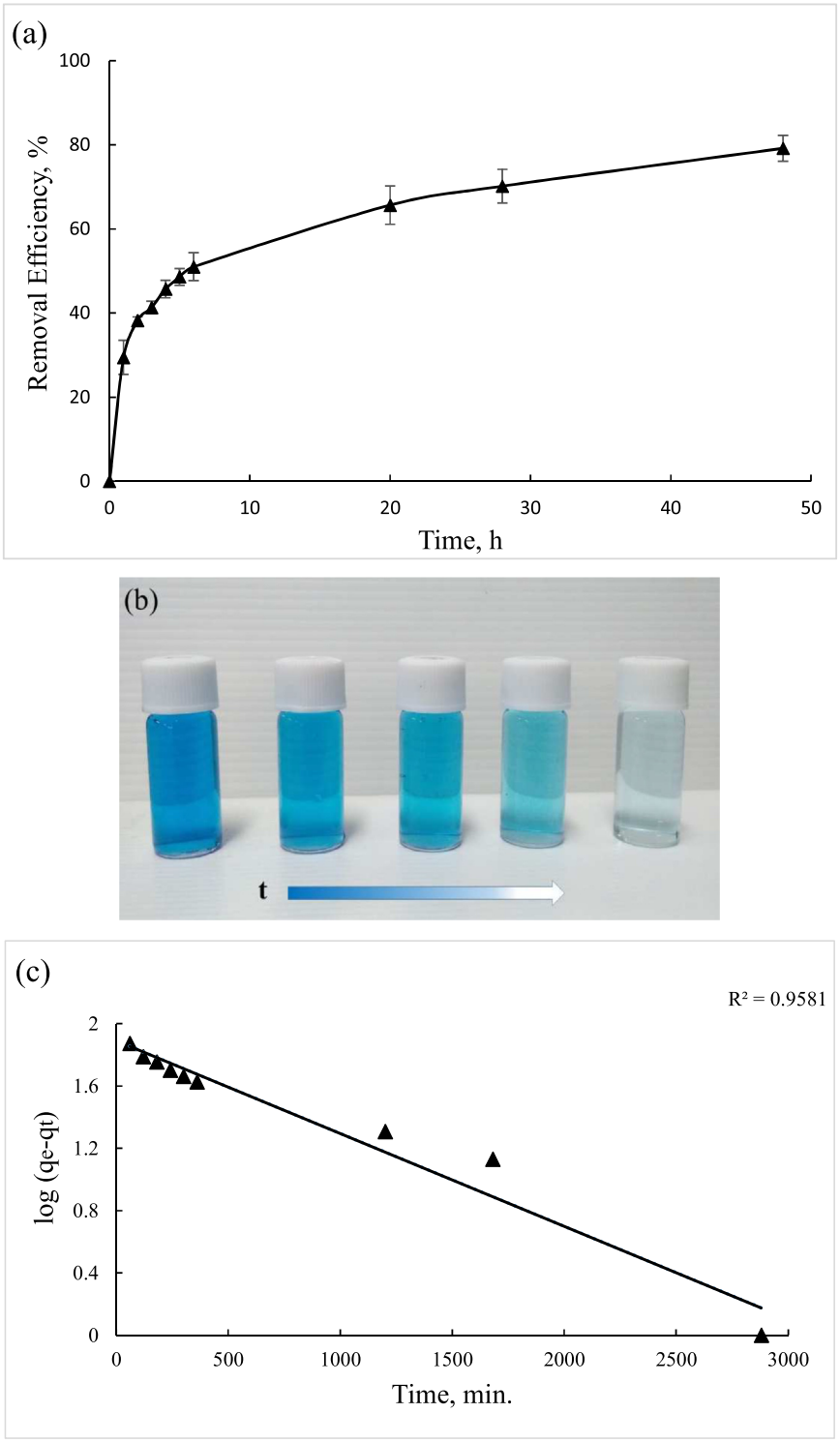

Fig. 8. Effect of contact time (a), digital photographs of MB dye solutions withdrawn at different time intervals (b), pseudo-first-order (c), pseudo-second-order (d), intra-particle diffusion (e) and Elovich (f) models for the adsorption of MB dye onto Chit/L_{NP}. (Experimental conditions: Chit/L_{NP}-based composite = 100 mg, dye concentration = 150 μg mL^{-1}, pH = natural, time range = 1–48 h, volume = 100 mL, shaking speed = 150 rpm; room temperature.)

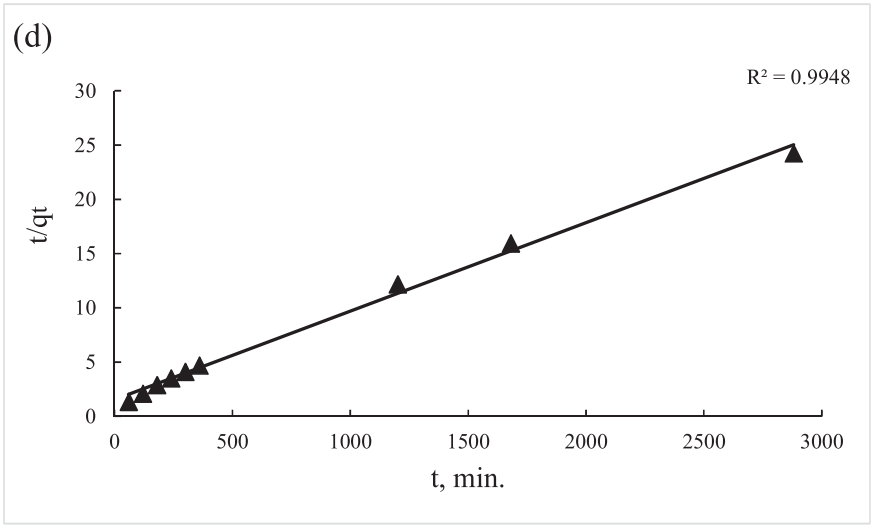

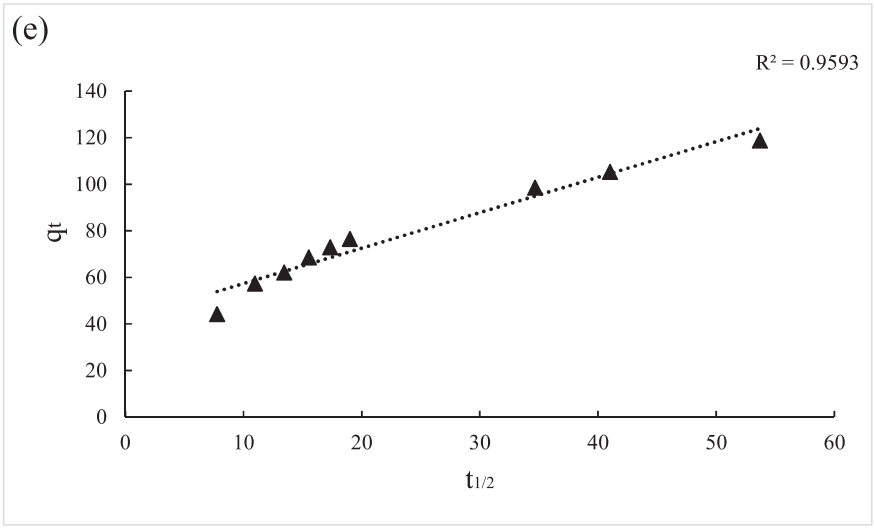

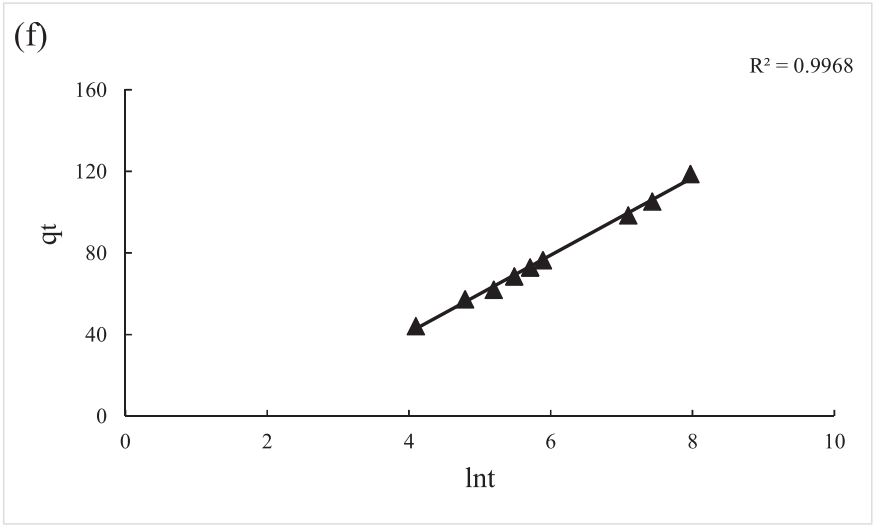

Fig. 8 (*continued*).

found to be 0.99 compared to the corresponding value representing pseudo-first order (0.96). The value of theoretical adsorption capacity (q_{max}, mg g^{-1}) derived from pseudo-second order model was in excellent agreement with the corresponding experimental value. This shows that pseudo-second order model better fitted the acquired kinetic data in present study. The graph between q_t and $t^{0.5}$ signifying intra-particle diffusion model is shown in Fig. 8e, where the value of 'C' which corresponds to the intercept helped in elucidating if controlling

Table 3
Comparison of pseudo-first-order, second-order-kinetic, intra-particle diffusion and Elovich models for model dye pollutant.

Kinetic model	Parameter	Value
Pseudo-first-order	q_{max} (mg g^{-1})	77.84
	K_1 (min^{-1})	0.001
	R^2	0.96
Pseudo-second-order	K_2 (g mg^{-1} min^{-1})	0.005
	q_{max} (mg g^{-1})	121.95
	R^2	0.99
Intra-particle diffusion model	K_{int} (mg g^{-1} $min^{-1/2}$)	1.5
	C (mg.g^{-1})	42.13
	R^2	0.96
The Elovich model	α (mg g^{-1} min^{-1})	120.30
	β (g mg^{-1})	0.053
	R^2	0.99

step is intra-particle diffusion or not. For present work, C was a non zero value (Table 3), showing that intra-particle diffusion is not the only rate-limiting step, but adsorption process also includes complex mechanism pathways [31]. The activation energy (β) of adsorption process elucidated from the Elovich model was much lower, which accords with excellent MB dye removal efficiency of Chit/L_{NP} composite material.

3.3.3. Effect of initial dye concentration on adsorption capacity of as-prepared composite

It can be seen from Fig. 9a that Chit/L_{NP} showed better adsorption capacity at lower MB dye concentration which indicated the presence adequate number of readily accessible active sites on the surface of composite material. However, adsorption capacity reached a steady value at relatively higher concentrations, suggesting that the interstitial spaces in the nanocomposite have become saturated. The Langmuir and Freundlich isotherms, and isothermal parameters for MB dye have been provided in Fig. 9b–c and Table 4, respectively. According to isotherm parameters given in Table 4, the Langmuir model better described the sorption of dye as obvious from R^2 values, signifying that monolayer adsorption played crucial role in the sorption of MB dye. The value of theoretical maximum of adsorption capacity (q_o) derived from Langmuir model was 74.07 mg g^{-1} for MB dye, which was in agreement with the corresponding experimental value, i.e., 71 mg g^{-1}. These values are better than the corresponding values of 36.25, 40.02, 33.78 and 26.69 mg g^{-1} for MB dye using activated lignin-chitosan extruded blends [17], organosolv lignin [45], magnetic lignin-based hollow microspheres [22] and ultrasonic surface modified chitin [46], respectively as sorbents. The comparison between different sorbents reported in literature with Chit/L_{NP} composite is provided in Table SI1 (see Supporting information).

3.3.4. Effect of temperature

Thermodynamic parameters for the sorption of MB dye onto Chit/L_{NP} composite were elucidated using the van't Hoff plots as provided in Table SI2 (see Supporting information). It is evident from the given data that sorption of MB increased with temperature, indicating that adsorption is an endothermic process as obvious from the positive value of ΔH^0 (14.40 kJ mol^{-1}). Besides, dye uptake was found to be a spontaneous process as confirmed from the negative value of $\Delta G°$. Besides, more negative values obtained at high temperature implied that dye uptake process was relatively higher at elevated temperature. Furthermore, it can be inferred from the positive value of ΔS^0 (0.049 kJ mol^{-1} K^{-1}) that there was increased randomness during the adsorption process at the solid/solution interface [31].

3.4. Comparative study

The performance of Chit/L_{NP} composite was compared to that of chitosan and chitosan-bulk lignin composite in terms of MB dye removal

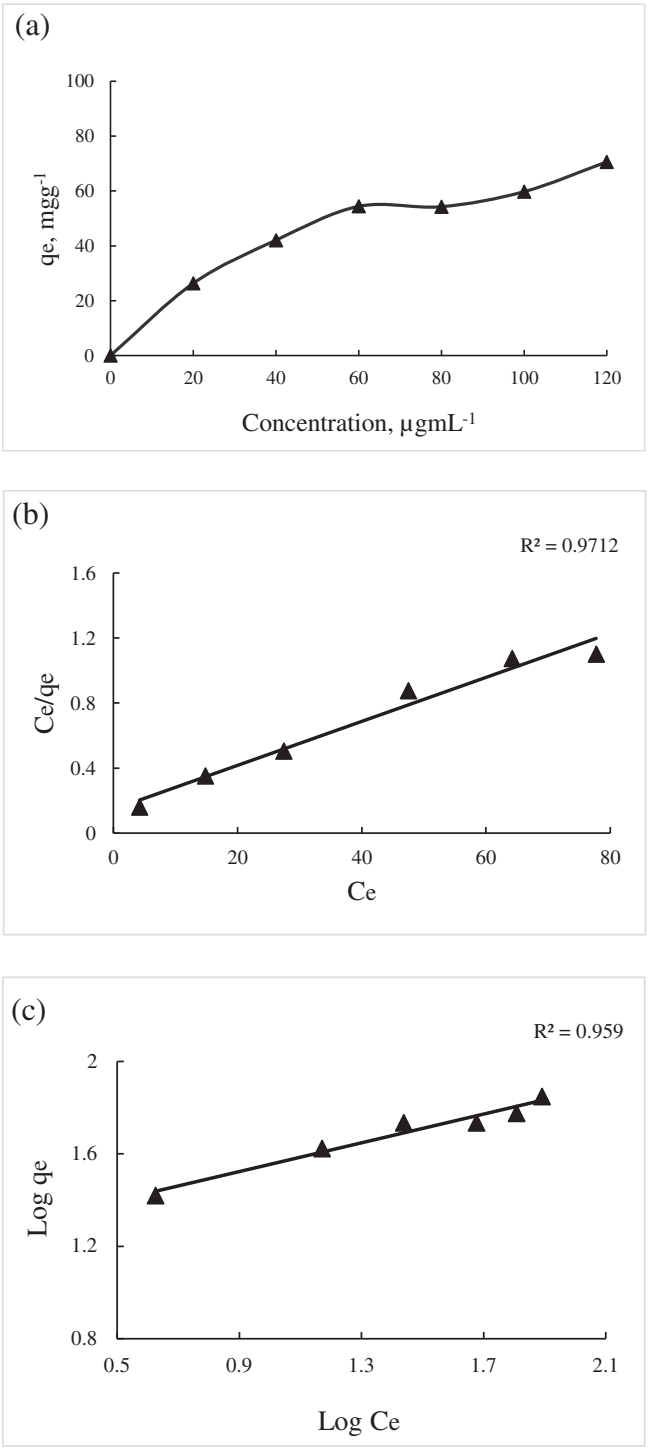

Fig. 9. (a) Effect of initial concentration of MB dye on adsorption capacity of Chit/L_{NP}.based composite. (b) Langmuir and (c) Freundlich models for MB dye. (Experimental conditions: Chit/L_{NP} = 15 mg, pH = natural, dye concentration range = 20–120 µg mL^{-1}, volume = 25 mL, shaking speed = 150 rpm, room temperature.)

efficiency to assess the influence of L_{NP} as additive in the resulting chitosan composite. It is clear from Fig. 10a that the bionanocomposite showed excellent removal efficiency for MB dye over extended pH range compared to other sorbents. As for L_{NP}, electron donor acceptor (EDA), i.e. π-π and n-π interactions between MB dye and L_{NP}, hydrogen bonding between hydrophilic oxygen-containing moieties coming from lignin distributed over composite material surface and that of MB dye molecules, π-hydrogen bonding interaction, electrostatic forces, and

Table 4
Comparison of different parameters of Langmuir and Freundlich isotherms for MB dye at 25 °C.

Adsorption isotherm	Parameter	Value
Langmuir	K_L (L mg^{-1})	0.092
	q_o (mg g^{-1})	74.07
	R^2	0.97
Freundlich	K_F ($mg^{1-1/n}$ $L^{1/n}$ g^{-1})	17.52
	N	3.22
	R^2	0.96

hydrophobic interactions together with their ultra-small size might have contributed towards imparting unusual adsorption properties to Chit/L_{NP} composite compared to bulk lignin.

3.5. Environmental applications

Another important aspect with regard to the practical utility and scale-up of sorbent material is the ability to remove target pollutants from real samples. Keeping this in view, a brief study was conducted to evaluate the performance of Chit/L_{NP} composite in terms of % removal efficiency using MB dye spiked real environmental aqueous samples: river water and tap-water. According to the results shown in Fig. 10b, Chit/L_{NP} composite demonstrated excellent dye decontamination from spiked samples, implying that developed adsorptive platform can be highly useful in wastewater treatment.

3.6. Desorption and reusability

To study these aspects, spent composite material was collected by filtration/decantation and later regenerated. In the next step, regenerated Chit/L_{NP} composite was used for sorption experiments in four successive cycles of adsorption-reuse. It is evident from the recyclability study given in Fig. SI5 (see Supporting information) that no marked decline in % MB dye removal was noticed. This suggested that Chit/L_{NP} composite was durable and has great potential as sustainable material for wastewater clean-up.

4. Conclusions

In the work described in this paper, we prepared lignin nanoparticles from palm kernel shell biomass residue and studied its application in fabricating a new lignin nanoparticles based chitosan nanocomposite (Chit/L_{NP}) for the removal of MB dye pollutant from aqueous solutions.

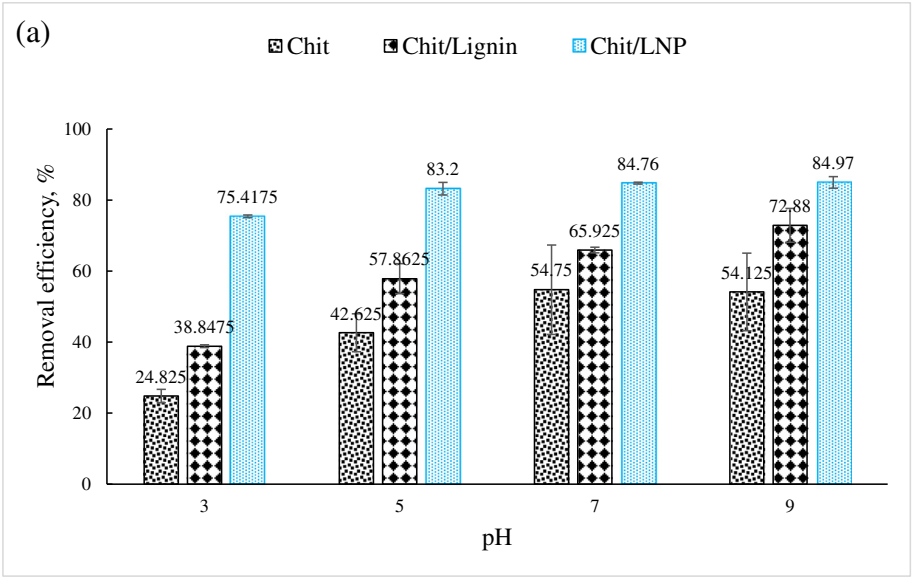

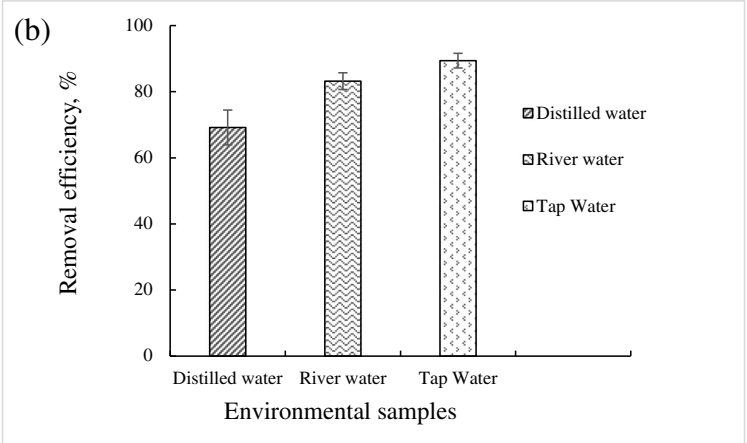

Fig. 10. (a) Comparison of MB dye removal efficiency of chitosan, chitosan-bulk lignin composite and Chit/L_{NP}. (Experimental conditions: sorbent = 10 mg, dye concentration = 20 μg mL^{-1}, volume = 25 mL, shaking speed = 150 rpm, room temperature.) (b) Evaluation of Chit/L_{NP} in removing MB dye from spiked real aqueous samples. (Experimental conditions: sorbent = 15 mg, dye concentration = 50 μg mL^{-1}, volume = 25 mL, shaking speed = 150 rpm, room temperature.)

Adsorption studies revealed that various factors including pH, contact time, dye concentration and temperature had influence on the removal of pollutant from their aqueous solutions. It was confirmed from experiments that the removal of dye from aqueous solution accorded well with pseudo-second-order kinetic model and the Langmuir isotherm model. In particular, the results of comparative study revealed that composite sorbent was highly efficient material in removing cationic MB dye. Overall, the strong interaction between dye molecule and chitosan/nano-lignin based composite could essentially be attributed to synergistic effects of size particularity (nano-range) and incorporated functionalities due to L_{NP} that led to enhanced uptake of dye pollutant from the test solutions. Studies on environmental application revealed that the matrix of spiked real water samples had essentially no adverse effect on dye uptake. In the continuity of this work, we advocate that new nano-lignin based green, sustainable, multifunctional and cheaper composite materials would be explored for application in advanced wastewater treatment systems.

Conflicts of interest

There are no conflicts of interest to declare.

Acknowledgements

The authors would like to acknowledge the financial support from Fundamental Research Grant Scheme (FRGS) by the Ministry of Education, Malaysia (grant no. FRGS 203/PTEKIND/6711525). Also, the Ministry of Education, Malaysia is acknowledged for the doctoral scholarship (MIS) awarded to Saima Sohni and Universiti Sains Malaysia for Postdoctoral fellowship awarded to Dr. Junidah Lamaming.

Appendix A. Supplementary data

Supplementary data to this article can be found online at https://doi.org/10.1016/j.ijbiomac.2019.03.151.

References

[1] D. Barana, M. Orlandi, L. Zoia, L. Castellani, T. Hanel, C. Bolck, R. Gosselink, Lignin based functional additives for natural rubber, ACS Sustain. Chem. Eng. 6 (9) (2018) 11843–11852.
[2] V.K. Thakur, M.K. Thakur, Recent advances in green hydrogels from lignin: a review, Int. J. Biol. Macromol. 72 (2015) 834–847.
[3] V.K. Thakur, M.K. Thakur, P. Raghavan, M.R. Kessler, Progress in green polymer composites from lignin for multifunctional applications: a review, ACS Sustain. Chem. Eng. 2 (5) (2014) 1072–1092.
[4] L. Dai, R. Liu, L.-Q. Hu, Z.-F. Zou, C.-L. Si, Lignin nanoparticle as a novel green carrier for the efficient delivery of resveratrol, ACS Sustain. Chem. Eng. 5 (9) (2017) 8241–8249.
[5] E. Larrañeta, M. Imízcoz, J.X. Toh, N.J. Irwin, A. Ripolin, A. Perminova, J. Domínguez-Robles, A. Rodríguez, R.F. Donnelly, Synthesis and Characterization of Lignin Hydrogels for Potential Applications as Drug Eluting Antimicrobial Coatings for Medical Materials, ACS Sustain. Chem. Eng. 6 (7) (2018) 9037–9046.
[6] W. Yang, J.M. Kenny, D. Puglia, Structure and properties of biodegradable wheat gluten bionanocomposites containing lignin nanoparticles, Ind. Crop. Prod. 74 (2015) 348–356.
[7] J. Chen, Y. Zhan, Y. Wang, D. Han, B. Tao, Z. Luo, S. Ma, Q. Wang, X. Li, L. Fan, Chitosan/silk fibroin modified nanofibrous patches with mesenchymal stem cells prevent heart remodeling post-myocardial infarction in rats, Acta Biomater. 80 (2018) 154–168.
[8] R. Hu, H. Zheng, J. Cao, Z. Davoudi, Q. Wang, Synthesis and in vitro characterization of carboxymethyl chitosan-CBA-doxorubicin conjugate nanoparticles as pH-sensitive drug delivery systems, J. Biomed. Nanotechnol. 13 (9) (2017) 1097–1105.
[9] Y. Yang, S. Wang, Y. Wang, X. Wang, Q. Wang, M. Chen, Advances in self-assembled chitosan nanomaterials for drug delivery, Biotechnol. Adv. 32 (7) (2014) 1301–1316.
[10] Q. Wang, Z. Dong, Y. Du, J.F. Kennedy, Controlled release of ciprofloxacin hydrochloride from chitosan/polyethylene glycol blend films, Carbohydr. Polym. 69 (2) (2007) 336–343.
[11] Q. Wang, Y.-m. Du, L.-h. Fan, H. Liu, X.-h. Wang, Structures and properties of chitosan-starch-sodium benzoate blend films [J], Wuhan Univ. J. (Nat. Sci. Ed.) 6 (2003) 013.
[12] F. Ali, S.B. Khan, T. Kamal, K.A. Alamry, A.M. Asiri, Chitosan-titanium oxide fibers supported zero-valent nanoparticles: Highly efficient and easily retrievable catalyst for the removal of organic pollutants, Sci. Rep. 8 (1) (2018) 6260.
[13] L. Chen, C.-y. Tang, N.-y. Ning, C.-y. Wang, Q. Fu, Q. Zhang, Preparation and properties of chitosan/lignin composite films, Chin. J. Polym. Sci. 27 (05) (2009) 739–746.
[14] V. Nair, A. Panigrahy, R. Vinu, Development of novel chitosan–lignin composites for adsorption of dyes and metal ions from wastewater, Chem. Eng. J. 254 (2014) 491–502.
[15] K. Crouvisier-Urion, P.R. Bodart, P. Winckler, J. Raya, R.g.D. Gougeon, P. Cayot, S. Domenek, F. Debeaufort, T. Karbowiak, Biobased composite films from chitosan and lignin: antioxidant activity related to structure and moisture, ACS Sustain. Chem. Eng. 4 (12) (2016) 6371–6381.
[16] K. Crouvisier-Urion, A. Lagorce-Tachon, C. Lauquin, P. Winckler, W. Tongdeesoontorn, S. Domenek, F. Debeaufort, T. Karbowiak, Impact of the homogenization process on the structure and antioxidant properties of chitosan-lignin composite films, Food Chem. 236 (2017) 120–126.
[17] A.B. Albadarin, M.N. Collins, M. Naushad, S. Shirazian, G. Walker, C. Mangwandi, Activated lignin-chitosan extruded blends for efficient adsorption of methylene blue, Chem. Eng. J. 307 (2017) 264–272.
[18] D. Kai, M.J. Tan, P.L. Chee, Y.K. Chua, Y.L. Yap, X.J. Loh, Towards lignin-based functional materials in a sustainable world, Green Chem. 18 (5) (2016) 1175–1200.
[19] S. Sohni, H. Nidaullah, K. Gul, I. Ahmad, A.M. Omar, nanotechnology for safe and sustainable environment: realm of wonders, Nanomaterials for Environmental Applications and their Fascinating Attributes, 2, 2018 37.
[20] W. Yang, E. Fortunati, F. Bertoglio, J. Owczarek, G. Bruni, M. Kozanecki, J. Kenny, L. Torre, L. Visai, D. Puglia, Polyvinyl alcohol/chitosan hydrogels with enhanced antioxidant and antibacterial properties induced by lignin nanoparticles, Carbohydr. polym. 181 (2018) 275–284.
[21] H. Stewart, M. Golding, L. Matia-Merino, R. Archer, C. Davies, Manufacture of lignin microparticles by anti-solvent precipitation: Effect of preparation temperature and presence of sodium dodecyl sulfate, Food Res. Int. 66 (2014) 93–99.
[22] Y. Li, M. Wu, B. Wang, Y. Wu, M. Ma, X. Zhang, Synthesis of magnetic lignin-based hollow microspheres: A highly adsorptive and reusable adsorbent derived from renewable resources, ACS Sustain. Chem. Eng. 4 (10) (2016) 5523–5532.
[23] A.P. Richter, B. Bharti, H.B. Armstrong, J.S. Brown, D. Plemmons, V.N. Paunov, S.D. Stoyanov, O.D. Velev, Synthesis and characterization of biodegradable lignin nanoparticles with tunable surface properties, Langmuir 32 (25) (2016) 6468–6477.
[24] J. Sameni, S. Krigstin, S.A. Jaffer, M. Sain, Preparation and characterization of biobased microspheres from lignin sources, Ind. Crop. Prod. 117 (2018) 58–65.
[25] W. Yang, E. Fortunati, D. Gao, G.M. Balestra, G. Giovanale, X. He, L. Torre, J.M. Kenny, D. Puglia, Valorization of acid isolated high yield lignin nanoparticles as innovative antioxidant/antimicrobial organic materials, ACS Sustain. Chem. Eng. 6 (3) (2018) 3502–3514.
[26] M. Lievonen, J.J. Valle-Delgado, M.-L. Mattinen, E.-L. Hult, K. Lintinen, M.A. Kostiainen, A. Paananen, G.R. Szilvay, H. Setälä, M. Österberg, A simple process for lignin nanoparticle preparation, Green Chem. 18 (5) (2016) 1416–1422.
[27] D. Tian, J. Hu, J. Bao, R.P. Chandra, J.N. Saddler, C. Lu, Lignin valorization: Lignin nanoparticles as high-value bio-additive for multifunctional nanocomposites, Biotechnol. Biofuels 10 (1) (2017) 192.
[28] S.K. Loh, The potential of the Malaysian oil palm biomass as a renewable energy source, Energy Convers. Manag. 141 (2017) 285–298.
[29] S. Sohni, N.A.N. Norulaini, R. Hashim, S.B. Khan, W. Fadhullah, A.K. Mohd Omar, Physicochemical characterization of Malaysian crop and agro-industrial biomass residues as renewable energy resources, Ind. Crop. Prod. 111 (2018) 642–650.
[30] X. Meng, A. Parikh, B. Seemala, R. Kumar, Y. Pu, P. Christopher, C.E. Wyman, C.M. Cai, A.J. Ragauskas, Chemical Transformations of Poplar Lignin during Cosolvent Enhanced Lignocellulosic Fractionation Process, ACS Sustain. Chem. Eng. 6 (7) (2018) 8711–8718.
[31] S. Sohni, K. Gul, F. Ahmad, I. Ahmad, A. Khan, N. Khan, S. Bahadar Khan, Highly efficient removal of acid red-17 and bromophenol blue dyes from industrial wastewater using graphene oxide functionalized magnetic chitosan composite, Polym. Compos. 39 (9) (2018) 3317–3328.
[32] O. Duman, S. Tunç, T.G. Polat, B.K. Bozoğlan, Synthesis of magnetic oxidized multiwalled carbon nanotube-κ-carrageenan-Fe3O4 nanocomposite adsorbent and its application in cationic Methylene Blue dye adsorption, Carbohydr.Polym. 147 (2016) 79–88.
[33] R.S. Fukushima, R.D. Hatfield, Extraction and isolation of lignin for utilization as a standard to determine lignin concentration using the acetyl bromide spectrophotometric method, J. Agric. Food Chem. 49 (7) (2001) 3133–3139.
[34] M. Wang, Y. Ma, Y. Sun, S.Y. Hong, S.K. Lee, B. Yoon, L. Chen, L. Ci, J.-D. Nam, X. Chen, Hierarchical Porous Chitosan Sponges as Robust and Recyclable Adsorbents for Anionic Dye Adsorption, Sci.Rep. 7 (1) (2017), 18054.
[35] K. Gul, S. Sohni, I. Ahmad, N. Ullah Khattak, R. Zada, N. Akhtar, N. Bahisht, Synthesis and Characterization of Graphene/Fe3O4 Nanocomposite as an Effective Adsorbent for Removal of Acid Red-17 and Remazol Brilliant Blue R from Aqueous Solutions, Curr. Nanosci. 12 (5) (2016) 554–563.
[36] S. Nethaji, A. Sivasamy, G. Thennarasu, S. Saravanan, Adsorption of Malachite Green dye onto activated carbon derived from Borassus aethiopum flower biomass, J. Hazard. Mater. 181 (1-3) (2010) 271–280.
[37] N. Umbreen, S. Sohni, I. Ahmad, N.U. Khattak, K. Gul, Self-assembled three-dimensional reduced graphene oxide-based hydrogel for highly efficient and facile removal of pharmaceutical compounds from aqueous solution, J. Colloid Interface Sci. 527 (2018) 356–367.
[38] K. Gul, S. Sohni, M. Waqar, F. Ahmad, N.N. Norulaini, M.O. AK, Functionalization of magnetic chitosan with graphene oxide for removal of cationic and anionic dyes from aqueous solution, Carbohydr. Polym. 152 (2016) 520–531.

[39] Y. Qian, Y. Deng, X. Qiu, H. Li, D. Yang, Formation of uniform colloidal spheres from lignin, a renewable resource recovered from pulping spent liquor, Green Chem. 16 (4) (2014) 2156–2163.
[40] F. Xiong, Y. Han, S. Wang, G. Li, T. Qin, Y. Chen, F. Chu, Preparation and formation mechanism of renewable lignin hollow nanospheres with a single hole by self-assembly, ACS Sustain. Chem. Eng. 5 (3) (2017) 2273–2281.
[41] A.H. Gedam, P.K. Narnaware, V. Kinhikar, Blended Composites of Chitosan: Adsorption Profile for Mitigation of Toxic Pb (II) Ions from Water, Chitin-Chitosan-Myriad *Functionalities in Science and Technology*, IntechOpen, 2018.
[42] H.M. Gad, A.A. El-Sayed, Activated carbon from agricultural by-products for the removal of Rhodamine-B from aqueous solution, J. Hazard. Mater. 168 (2) (2009) 1070–1081.
[43] Q. Peng, M. Liu, J. Zheng, C. Zhou, Adsorption of dyes in aqueous solutions by chitosan–halloysite nanotubes composite hydrogel beads, Microporous Mesoporous Mater. 201 (2015) 190–201.
[44] L. Zeng, M. Xie, Q. Zhang, Y. Kang, X. Guo, H. Xiao, Y. Peng, J. Luo, Chitosan/organic rectorite composite for the magnetic uptake of methylene blue and methyl orange, Carbohydr. Polym. 123 (2015) 89–98.
[45] S. Zhang, Z. Wang, Y. Zhang, H. Pan, L. Tao, Adsorption of methylene blue on organosolv lignin from rice straw, Procedia Environ. Sci. 31 (2016) 3–11.
[46] G. Dotto, J. Santos, I. Rodrigues, R. Rosa, F. Pavan, E. Lima, Adsorption of Methylene Blue by ultrasonic surface modified chitin, J. Colloid Interface Sci. 446 (2015) 133–140.